ECS Journal of Solid State
Science and Technology

Film Characterization of Low-Temperature Silicon Carbon Nitride for Direct Bonding Applications

ECS Journal of Solid State Science and Technology, 2020 **9** 123011

Film Characterization of Low-Temperature Silicon Carbon Nitride for Direct Bonding Applications

F. Nagano,[1,2,*,z] S. Iacovo,[2] A. Phommahaxay,[2] F. Inoue,[2,] E. Sleeckx,[2] G. Beyer,[2] E. Beyne,[2] and S. De. Gendt[1,2,***]**

[1]*Department of Chemistry, KU Leuven, 3001 Leuven, Belgium*
[2]*Imec, 3001 Leuven, Belgium*

Silicon carbon nitride (SiCN) compounds have aroused great interest as dielectric materials for direct bonding because of the high thermal stability and high bond strength, as well as its Cu diffusion barrier properties. While wafer-to-wafer direct bonding, including the dielectric deposition step, is generally performed at high temperature (>350 °C), applications such as heterogeneous chips and DRAMs would require wafer-to-wafer direct bonding at lower temperature (<250 °C). In this study, we evaluate, for SiCN deposited at various temperatures, the impact for direct wafer bonding of lowering the temperature of all processes. Chemical and mechanical properties of SiCN direct bonding are studied.

 [DOI: 10.1149/2162-8777/abd260]

Manuscript submitted September 3, 2020; revised manuscript received November 5, 2020. Published December 23, 2020. *This was Paper 1650 presented during PRiME 2020, October 4–9, 2020.*

Two-dimensional circuit scaling is becoming problematic because of footprint limitations and high development cost. Three-dimensional (3D) circuit integration using a vertical stack offers benefits of shorter interconnects, allows heterogeneous integration, and lowers the production cost compared to usage of 2D scaling technology.[1,2] Generally, solder base micro bump connections have been developed and applied as the interconnect for 3D integration.[2–7] Stacking issues arise for pitch less than 2 μm, due to micro bump alignment tolerance during thermal compression bonding. In addition, void defects in micro bumps, induced by electromigration between solder and Cu, are becoming detrimental for finer pitch. Consequently, wafer-to-wafer direct bonding attracts interest as one of the promising strategies to achieve not only 3D integration benefits, but it also allows high productivity and high accuracy integration.[8–12] The planar system-on-chip (SoC) can be connected to the back-end-of-line (BEOL) layer through wafer-to-wafer direct bonding allowing high-density interconnection applications with shorter Through-Si-Vias (TSV).[9,13] Surface plasma activated bonding has received attention as the most applicable method to gain high bond strength and reduce the thermal budget for CMOS process. Surface activated bonding and chemical mechanical polishing (CMP) processes were combined to provide ultra-smooth surfaces, as such direct bonding without adhesive materials can be processed at room temperature while maintaining ultra-fine pitch and high accuracy in wafer-to-wafer stacking.[14–21] In this direct bonding scheme, two different concepts are considered–one is homogeneous bonding as required for 3D sequential integration using dielectric-to-dielectric and TSVs, and the other is hybrid bonding based on Cu-to-Cu, Cu-to-dielectric, and dielectric-to-dielectric simultaneously bonding. For these bonding structures, dielectric material adjacent to Cu is required to serve not only as an insulator, but also as a mechanical buffer to withstand the grinding process for further 3D integration. Plasma surface activation of the bonding surface is the most reported method in the literature about wafer-to-wafer direct bonding options to gain high bond strength and reduce the thermal budget for CMOS processes.[22,23]

Although SiO_2–SiO_2 bonding is historically studied for wafer-to-wafer direct bonding development, it is reported that SiO_2-SiO_2 bonding is hampered due to out-gassing at the bonding interface after post-bond annealing. Moreover, SiO_2 is known as a less suitable dielectric against Cu diffusion. In our previous reporting,[2,20,21] it was seen that SiCN is a promising alternative dielectric as it possesses essential properties such as high bond strength at lower annealing temperature conditions. In addition, even though SiCN bond annealing was performed at higher temperatures than the deposition temperature, no out-gassing at the interface was observed.

SiCN films for hybrid bonding are generally fabricated by plasma enhanced chemical vapor deposition (PECVD) at high temperature (>350 °C). Following post-bond annealing (<250 °C), the bond strength of SiCN can reach over 2.0 J m^{-2} after direct bonding at room temperature.[8] For some applications like DRAM however, there are more stringent temperature requirements for back-to-face wafer-to-wafer hybrid bonding, that is the deposition temperature of the current SiCN films, exceeds the memory assembly thermal budget (<250 °C). Therefore, to achieve such a back-to-face bonding, the SiCN films as back-side bonding layer are expected to be deposited at lower temperatures (<250 °C). Therefore, low-temperature deposition and processing of SiCN should be investigated and properties of wafer-to-wafer direct bonding with SiCN deposited at lower temperature needs to be evaluated. In this paper, wafer-to-wafer direct bonding properties with SiCN deposited at varying temperatures are evaluated in terms of bonding uniformity and strength. The impact on film properties of each SiCN process step is studied by using specific characterization techniques.

Experimental

In this study, 300 mm Si wafers were used for wafer bonding experiments. The SiCN films were deposited by plasma enhanced chemical vapor deposition (PECVD). SiCN films were deposited at 200 °C (which will be indicated as SiCN 200 °C in the text) as well as with the standard SiCN process temperature of 370 °C (indicated as SiCN 370 °C). Deposition precursors are NH_3 and $SiH_x(CH)_y$. Deposition thickness was targeted for 120 nm thickness and verified with spectroscopic ellipsometry. After deposition, these wafers were annealed for 10 min in a 10% H_2/N_2 atmosphere at a temperature of 400 °C for SiCN 370 °C, while a temperature of 200 °C was applied for SiCN 200 °C. Subsequently, a CMP process with typical barrier metal slurry and pad was employed to smoothen the SiCN surface. Next, the wafer surface was activated by using an N_2 plasma in the EVG GEMINI system and rinsed in deionized water. Wafers were then finally bonded at room temperature without bonding pressure in the EVG GEMINI system. Different characterization techniques have been used to understand the layer quality of both SiCN

*Electrochemical Society Student Member.
**Electrochemical Society Member.
***Electrochemical Society Fellow.
[z]E-mail: Fuya.Nagano@imec.be

processes. The thickness of the SiCN films deposited on the Si wafer was measured by Spectroscopic Ellipsometry (F5-SCD, Kla-Tencor) by observing and fitting the change in polarization of reflected light. The mass of the SiCN films as deposited on the Si wafer was measured with a mass measurement tool (Mentor DF3, Metryx) with sensitivity in the microgram level. The elemental composition of the dielectric films was studied by elastic recoil detection (ERD, Giangrandi 2007) at 8 MeV using Cl^{4+}. Fourier transform infrared spectroscopy (FTIR, Nicolet 6700) was carried out in the wave number range of 400–4000 cm^{-1} to investigate the chemical bonds. During the FTIR, the optical part of the spectrometer was evacuated, and baseline correction was done to compensate for the remaining absorption bands of air components, H_2O and CO_2 by analysis software (OMNIC 9, Thermo Fisher Scientific). Atomic force microscope (AFM, dimension 3100, Bruker) was performed to determine surface roughness. X-ray photoelectron spectroscopy (XPS, Theta300, Thermo Instruments) was applied to study the chemical bonds at the dielectric surface and bulk. The bonding uniformity was inspected by using Scanning Acoustic Microscopy (SAM, PVA Tepla SAM300 AutoWafer). After the first SAM inspection, all bonded wafer pairs are subject to a post-bond annealing (PBA) at 250 °C for 2 h in N_2 ambient to obtain solid bonding strength. Bonding strength energy after PBA was calculated from the results using the blade insertion method. All experiments were executed multiple times to obtain statistical information. The cross-sectional images were obtained by transmission electron microscopy (TEM, FEI Tecnai F30). Energy dispersive X-ray analysis was employed together with TEM to identify chemical composition of the intermediate layer.

Result and Discussion

SiCN film characterization.—Table I shows a summary of the properties of SiCN 370 °C and 200 °C deposited on the Si wafers. From the measured thickness and weight of the deposited SiCN, the density for the SiCN films was extracted. The average value of actual thickness was extracted as 119.3 nm for SiCN 370 °C and 166.3 nm for SiCN 200 °C based on 21 measurement spots by spectroscopic ellipsometry on selected wafers. In addition, the weight of each SiCN deposited on the Si wafer was measured as 17.4 mg for SiCN 370 °C and 15.6 mg for SiCN 200 °C. Young's modulus of SiCN 200 °C and 370 °C was measured by nano-indentation. The refractive index and the density demonstrate the expected correlation. The SiCN 200 °C is likely less dense compared to SiCN 370 °C, meaning that a different structure of SiCN is formed due to the low temperature deposition.

Figure 1 shows the elemental composition mapping as a function of film thickness as collected with ERD. The elemental composition at a depth of 50–70 nm are shown in Table II. Although the SiCN 370 °C contains only Si, C, N and H, SiCN 200 °C is characterized by the presence of oxygen into the bulk and a slightly higher C content compared to SiCN 370 °C, identifying the material as SiCNO and not pure SiCN. The deposition chamber in PECVD process used in this experiment can maintain high vacuum levels. Furthermore, no oxygen containing precursors are purged in the PECVD process with 10% N_2/H_2, while also the used precursors should not result in oxygen inclusion in the material matrix. Therefore, the likely source of oxidizing species is the ambient and moisture at which the wafers are exposed after deposition. While SiCN 370 °C shows oxidation only on the top surface, SiCN 200 °C is oxidized through the entire bulk. Possible reasons relate to the lower density of SiCN 200 °C which allows ambient molecules to penetrate more easily within the layer. In addition, the SiCN 200 °C may have remaining precursor bonds, as discussed in the following section.

Figure 2 shows the FTIR absorbance spectra of SiCN 370 °C and SiCN 200 °C. The detected peaks in the FTIR spectra are mainly assigned to the vibration modes described in Table III.[24–31] In Fig. 2, the broad peaks at 3100–3500 cm^{-1} are attributed to O–H presence in the film, indicating moisture absorption from air ambient and being more pronounced for the SiCN 200 °C. In addition, the peak of Si–O strongly appears in the 800–1200 cm^{-1} region for SiCN 200 °C. This confirms that oxygen or moisture coming from air ambient reacts with Si atoms in the less dense SiCN matrix. These samples were analysed by FTIR again after 3 months storage in cleanroom ambient. For SiCN 370 °C, no apparent differences of the film are visible after 3 months storage. While for SiCN 200 °C, Si–CH_3 peak slightly decreased and Si–O peak became more significant compared to the as-deposited SiCN 200 °C. This means that SiCN 200 °C oxidized further by absorbed moisture or oxygen reacting with residual precursor after 3 months storage in air ambient. A peak at $\sim$1160 cm^{-1} can be assigned to Si-CH_3. For SiCN 200 °C, the appearance of the strong Si-CH_3 peak suggests that unreacted precursor remains in the film. A peak of C-H positioned in the 2700–3100 cm^{-1} can be expected to also relate to Si-CH_3, also supporting the presence of unreacted precursor residues.

Figure 3 shows XPS spectra on the surface of SiCN 370 °C and SiCN 200 °C. For N1s spectra, typically the 396.6, 398.9 eV, and 399.3 eV positions are attributed to the N-Si, N-C, and NH_3, respectively. Based on the XPS measurements of the N1s peak of SiCN 200 °C, the peak at 393.3 eV is assumed to relate to NH_3, while no similar peak, thus NH_3 peaks can be detected from the as-deposited SiCN 370 °C. This is suggesting further the presence of residues of deposition precursors in SiCN 200 °C and likewise consistent with the appearance of Si-CH_3 peaks in the resulting FTIR spectra. Therefore, it is concluded that the SiCN 200 °C film is stoichiometrically unstable. In addition, the XPS spectra in Fig. 3 have no apparent indications of N–C bonds around the specific bonding energy region (398.9 eV). Figure 4 shows the XPS spectra for the C1s on the surface of SiCN 370 °C and SiCN 200 °C. For C1s spectra, the 282.1, 284.1, and 286.5 eV peaks are attributed to the C–Si, C–C, and C–N, respectively. The main peak visible in the spectra of SiCN 370 °C and SiCN 200 °C is composed of C–Si and C–C bonds, while no significant peaks for C–N bonds are confirmed from the fitting for either SiCN 370 °C and SiCN 200 °C in the C1s spectra. Therefore, since NH_3 and Si-CH_x based precursors were used in this study for the SiCN deposition, the layers are assumed to be composed of C–C and Si–C bonds with little to no C–N bond formation. This is also confirming that the significant peaks assigned to C–N bonds are not observed in the reported FTIR spectra in Fig. 2.

In the bonding sequence, after deposition, the SiCN 370 °C and SiCN 200 °C were polished using a CMP process. Surface smoothness has been measured by AFM. Table IV shows arithmetic averages of the roughness profile, R_a, for both SiCN 370 °C and 200 °C. R_a was obtained as 0.36 nm and 0.42 nm for both SiCN 370 °C and 200 °C before CMP. The ultra-smooth are then obtained by CMP, which R_a was given as 0.09 nm and 0.11 nm for SiCN 370 °C and 200 °C. Even after N_2 plasma activation the surface smoothness was maintained with the R_a of 0.09 nm and 0.11 nm for SiCN 370 °C and 200 °C. This is suggesting little possibilities for defect generation due to the surface roughness in the direct bonding.

Table I. Film properties for each SiCN as-deposited film.

	Refractive index, -	Thickness, nm	Weight, mg	Density, g cm^{-3}	Young's modulus, GPa
SiCN 370 °C	2.04	119.3 ± 1.4	17.4	1.85 ± 0.02	90.0 ± 5.0
SiCN 200 °C	1.61	166.3 ± 1.9	15.6	1.32 ± 0.02	12.5 ± 1.1

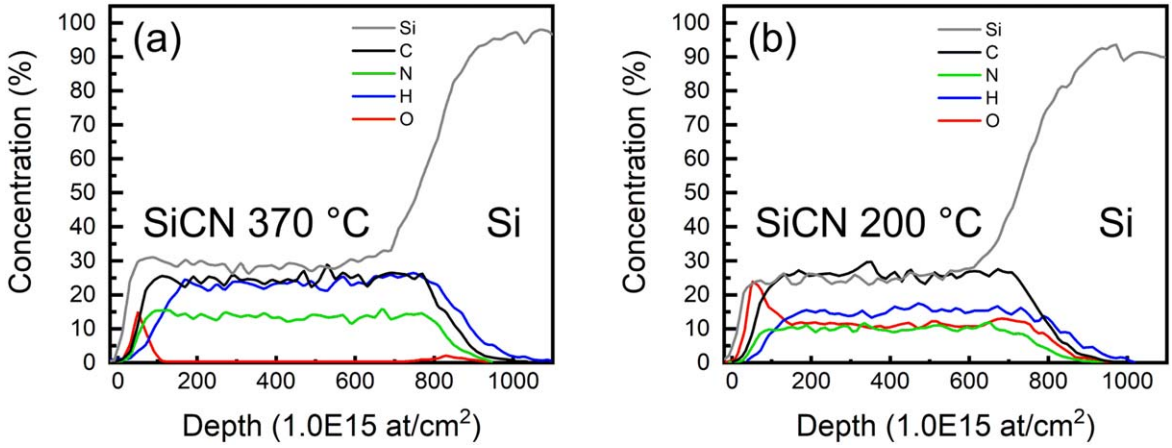

Figure 1. Elemental composition of as deposited SiCN films as obtained by ERD depth profile for (a) SiCN 370 °C deposition, (b) SiCN 200 °C deposition. Uncertainties are ~7.5 % for the major constituent (>15 at%), ~10 % for the minority constituent (<15 at%), and ~20 % for hydrogen more than 10 at%.

Table II. Elemental composition of SiCN as-deposition films positioned at 50–70 nm depth. Uncertainties are ~7.5% for the major constituent (>15 at%), ~10 % for the minority constituent (<15 at%), and ~20% for hydrogen more than 10 at%.

	Atomic composition, %					Empirical formula
	Si	C	N	H	O	
SiCN 370 °C	31.6	27.6	15.1	25.8	0	Si 1 C 0.87 N 0.48 O 0.00 H 0.82
SiCN 200 °C	28.2	30.1	11.5	17.4	12.7	Si 1 C 1.07 N 0.41 O 0.45 H 0.61

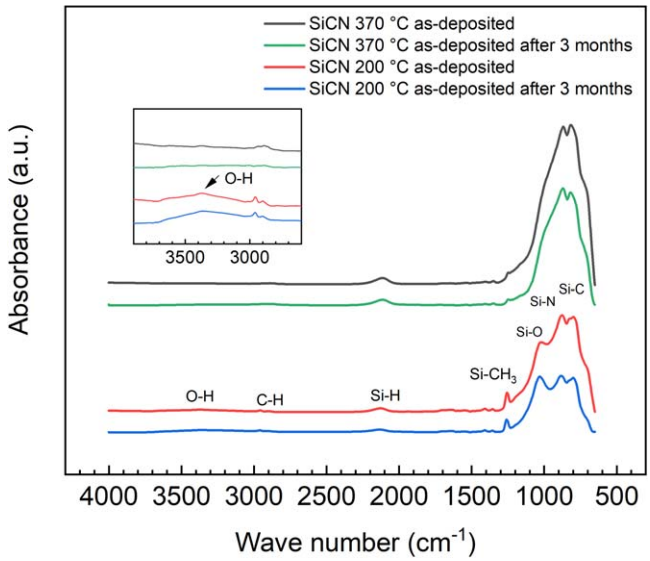

Figure 2. Absorbance mode spectra of FTIR for SiCN 370 °C as-deposited and 200 °C as-deposited.

Figure 5 shows the spectra of XPS in the Si2p region before and after N_2 plasma for SiCN 370 °C and SiCN 200 °C. For Si 2p spectra, the 100.4, 101.9 and 102.5 eV peaks are attributed to the Si–C, Si–N and Si–O bonds, respectively. From Fig. 5a, a Si–C peak and mixed peak of Si–N and Si–O before N_2 plasma activation for the SiCN 370 °C were observed at the surface. After N_2 plasma activation Si–C peak is decreasing for SiCN 370 °C. It might be that the plasma process is breaking bonds, creating Si and C dangling bonds, as suggested in previous studies.[20,21] On the other hand, it is found that SiCN 200 °C has initially much lower amount of Si–C bonds as shown in Fig. 5. It is possible to observe that while for SiCN 370 °C the contribution of Si–C bonds to the main peak is significant (Fig. 5a), for SiCN 200 °C we can barely see a peak corresponding to Si–C bonds (Fig. 5b). As it was demonstrated that Si and C dangling bonds are essential in the process of enhancing bond energies, the absence of this signature indicates that the desired film properties for good bonding are lacking.[20,21]

To clarify the plasma impact on the surface Si–N bonds, the surface sensitive XPS analysis in the N1s region was performed before and after N_2 plasma for SiCN 370 °C and SiCN 200 °C (Fig. 6). For N1s spectra, the main peak located at 397.3 eV is attributed to N–Si bonds. For SiCN 370 °C, the significant N-Si peak is visible in the N1s spectra. While for SiCN 200 °C, the N-Si peak is weaker compared to SiCN 370 °C. This is confirmed in the Si2p spectra shown in Fig. 6b, the contribution of Si–N bonds to the main peak is relatively small for SiCN 200 °C and Si–O bonds are dominant. After N_2 plasma, most of the surface N–Si bonds are removed for both SiCN 370 °C and SiCN 200 °C. Considering the Si2p spectra in Fig. 5, it is concluded that N_2 plasma terminates not only the Si–C bonds but also Si–N bonds on the surface of SiCN. Si–O bonds are expected to be formed for SiCN 370 °C and SiCN 200 °C after wafers were exposed to air ambient after N_2 plasma treatment.

Wafer-to-wafer bonding characterization.—To evaluate the impact of differences between both SiCN growth conditions, bonding uniformity for bonded wafer pairs of SiCN 370 °C and 200 °C have been inspected by SAM. There are no visible voids after room temperature bonding. After the first SAM inspection, these bonded wafers were subjected to post-bond annealing (PBA) at 250 °C for 2 h to obtain solid bond strength. After PBA all wafer pairs were inspected again by SAM and again no voids at the interface are observed for either SiCN 370 °C and 200 °C.

Bond energies for the different wafer pairs have been calculated by using the blade insertion method. Figure 7 shows the result of bond energy for SiCN 370 °C and 200 °C. The highest bond energy $\sim$ 2.3 J m^{-2} was obtained in the case of SiCN 370 °C, while the bond energy for SiCN 200 °C was $\sim$1.4 J m^{-2}. The latter values are not sufficient to survive mechanical process (e.g. grinding and

Table III. Peak positions of infrared absorption for the SiCN film.[24–29]

Peak position, cm^{-1}	Vibration mode
830	Si–C
940	Si–N
1025	Si–O
1110	C–H
1120	C–N
1160	$N–H_x$
1260	$Si–CH_3$
1200–1700	C=N
2100	Si–H
2200	C≡N
2700–3100	C–H in CH_3
3100–3500	O–H

for bonded wafer pairs after wafer thinning on top wafer.[32,33] Figure 8 shows high angle annular dark field STEM (HAADF-STEM) of the bonding interface of SiCN 370 °C and 200 °C. For the case of SiCN 370 °C shown in Fig. 8a, a clear intermediate layer was observed with a thickness of 7.0 nm. On the other hand, for the case of SiCN 200 °C in Fig. 8b, a twice as thick intermediate layer with a graded interface was observed compared to that of SiCN 370 °C. The latter is assumed to be related to the less dense nature of the film, allowing absorbed moisture into the film to generate the intermediate layer. The thicker oxidized layer was then formed for SiCN 200 °C by the reaction between absorbed moisture and incomplete SiCN film during post-bond annealing with the temperature of 250 °C. The different contrast layers observed in Fig. 8 were analyzed by EDS. Figure 9 shows EDS analysis for bonding interface of SiCN 370 °C and 200 °C. For SiCN 370 °C shown in Fig. 9a, at the bonding interface the amount of carbon and nitrogen atoms dramatically decreased while also oxygen atoms were detected, although not observed in the FTIR analysis. This is

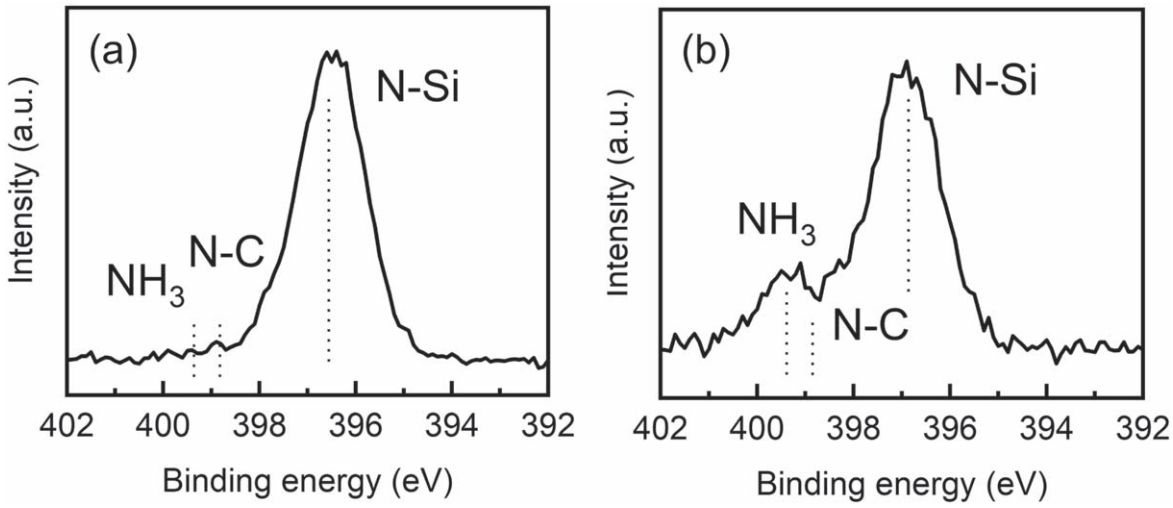

Figure 3. XPS spectra (21 degree-angle from normal) in the N1s for (a) SiCN 370 °C as-deposited and (b) SiCN 200 °C as-deposited.

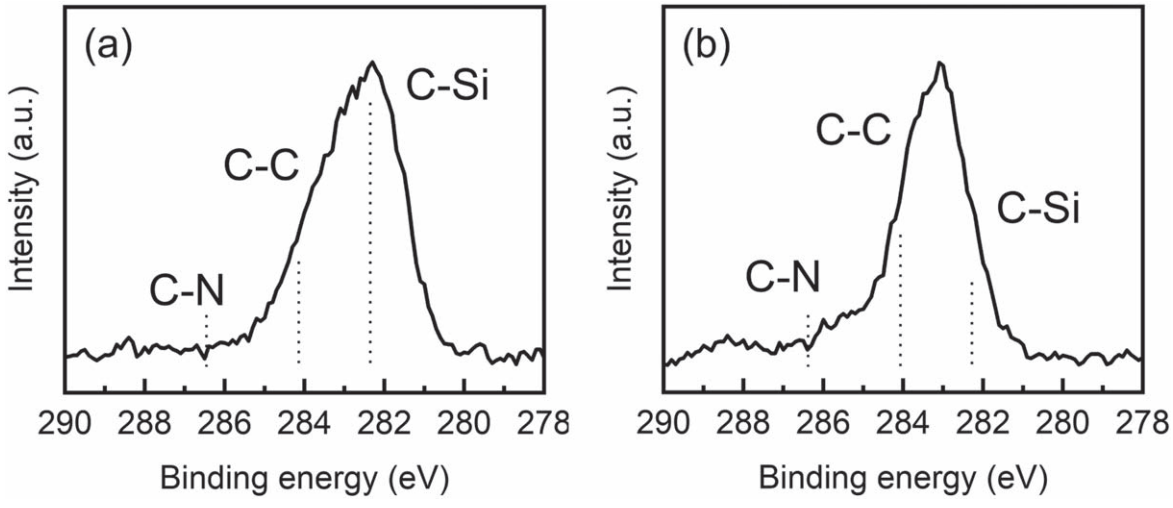

Figure 4. XPS spectra (21 degree-angle from normal) in the C1s for (a) SiCN 370 °C as-deposited and (b) SiCN 200 °C as-deposited.

dicing) conditions required after bonding. It may induce slippage or delamination of the bonded wafer since the lowest bonding energy for which we verified mechanical stability was $\sim 1.8\ J\ m^{-2}$.[20]

In order to elucidate the differences in bond strength, we examined the interface structure, i.e. TEM and EDS were performed expected to relate to an oxidized layer since it has also been reported in past studies that an oxidized intermediate layer at the bonding interface of SiCN is formed.[21] For SiCN 200 °C shown in Fig. 9b, oxygen presence was detected by ERD. At the center of intermediate layer, it matches the stoichiometry of SiO_2. Therefore, at the

Table IV. Roughness of SiCN films before and after CMP, and after N_2 plasma.

	Roughness (R_a), nm		
	Before CMP	After CMP	After N_2 plasma
SiCN 370 °C	0.36	0.09	0.09
SiCN 200 °C	0.42	0.11	0.11

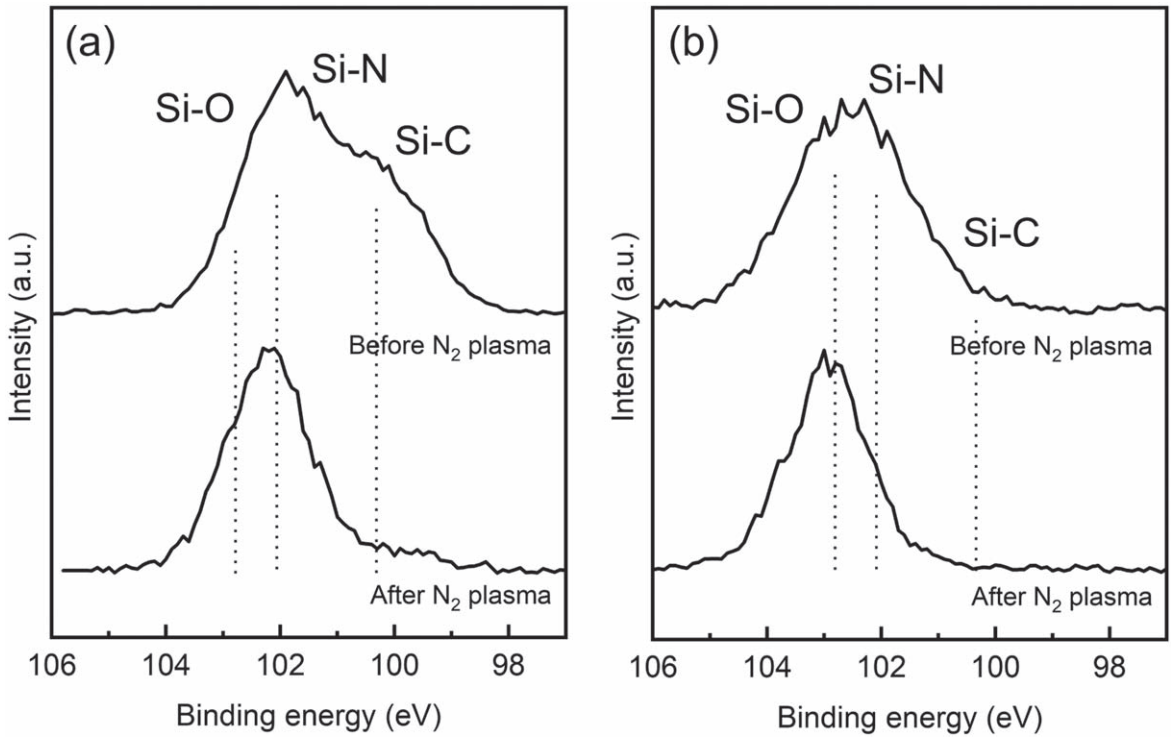

Figure 5. Spectra of XPS (78 degree-angled) in the Si2p peaks for: (a) SiCN 370 °C before and after N_2 plasma, (b) SiCN 200 °C before and after N_2 plasma.

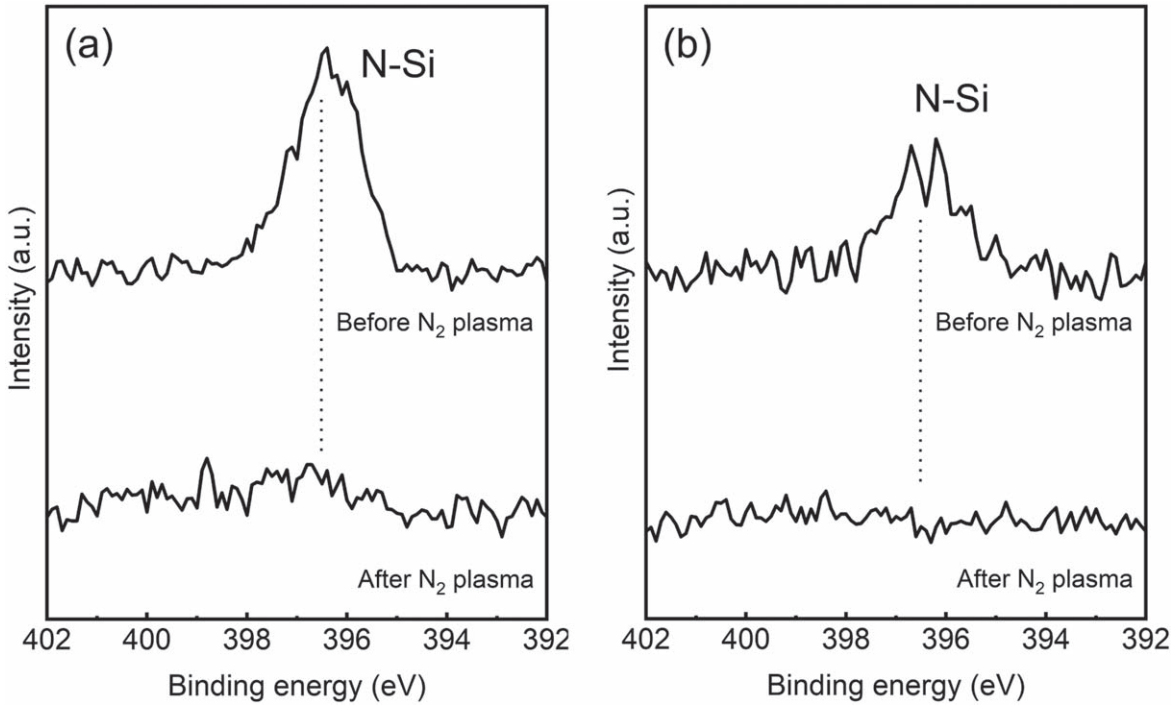

Figure 6. Spectra of XPS (78 degree-angled) in the N1s peaks for: (a) SiCN 370 °C before and after N_2 plasma, (b) SiCN 200 °C before and after N_2 plasma.

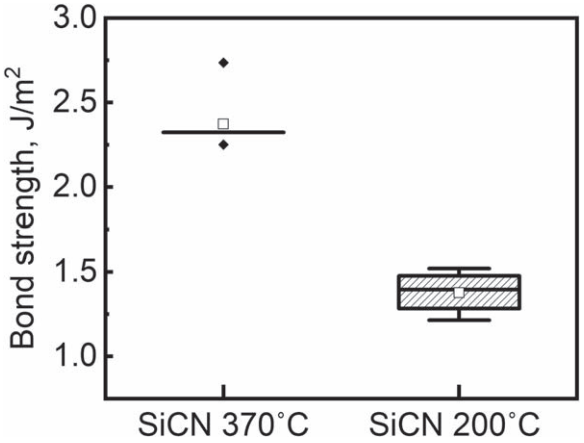

Figure 7. Bond energies for all the SiCN samples with specific process temperature.

structure of SiCN 200 °C, such a mixed situation of the film explains the weaker bond strength compared to SiCN 370 °C. ERD analysis revealed that a at PDA 200 °C or PBA 250 °C do not change the observed process observations. In summary, it is found that the appropriate deposition process of the SiCN film is essential for good quality bonding. The latter in combination with CMP and plasma activation to keep the quality of wafer-to-wafer dielectric bonding in the case of SiCN. For low temperature deposition of SiCN film, the optimization of the precursor or film modification process has to be studied further.

Conclusions

PECVD SiCN films were deposited at 370 °C and 200 °C and the bonding process after full wafer-to-wafer direct bonding processes was evaluated. Specific measurements for surface and bonding properties like ERD, FTIR, XPS, AFM, SAM, blade insertion, TEM, and EDS were performed. By chemical composition analysis, the presence of oxygen was observed for SiCN 200 °C. FTIR and XPS results showed that the components, Si-CH_3 and NH_3, assigned

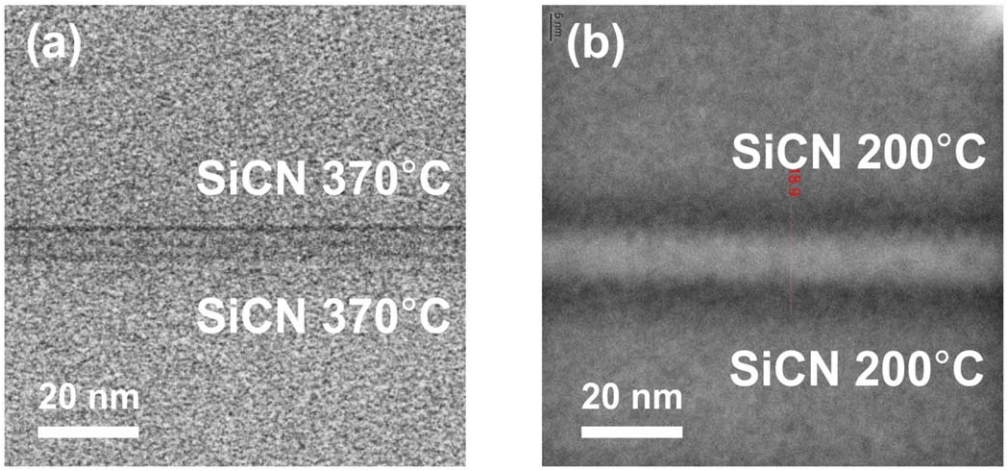

Figure 8. TEM of bonding interface after 250 °C post bond annealing for (a) SiCN 370 °C and (b) 200 °C.

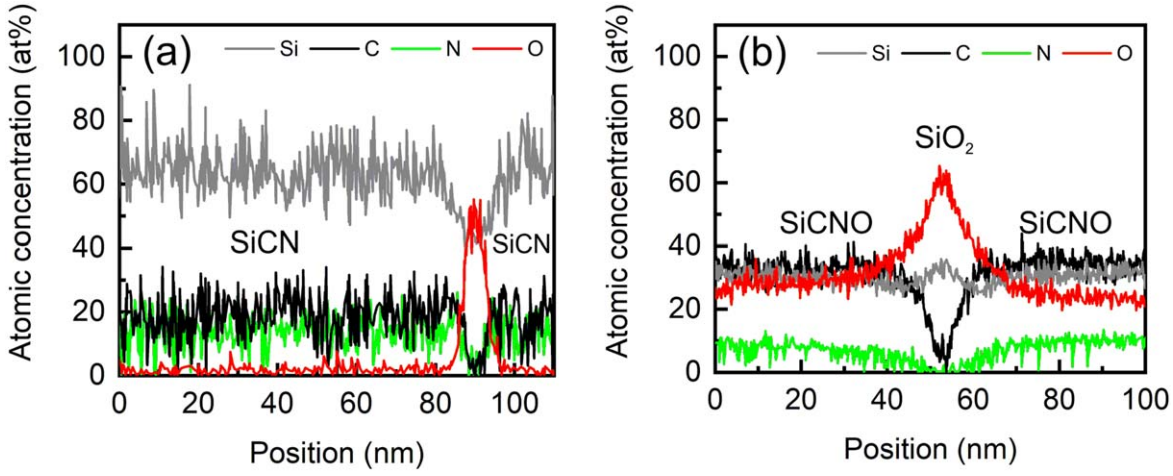

Figure 9. EDS analysis of bonding interface for (a) SiCN 370 °C and (b) SiCN 200 °C.

interface for the SiCN 200 °C likely a more SiO_2 to SiO_2 bonding occurs. We have demonstrated that the bond energy of SiO_2 to SiO_2 direct bonding is ~1.7 J m^{-2} in past study.[2] In addition, the interface has graded composition of carbon, nitrogen, and oxygen. This indicates that the interface of SiCN 200 °C has the mixed intermediate layer of SiO_2 and SiCNO. Considering the less dense film to residual precursor remain in SiCN 200 °C film due to low temperature deposition and reacted with absorbed moisture in air, indicating the incomplete and unstable film. Before N_2 plasma activation much fewer Si–C bonds were observed for the surface of SiCN 200 °C film compared to SiCN 370 °C film. Although only a certain amount of Si–C bonds was terminated on the surface of SiCN

370 °C by N_2 plasma activation, it was observed that the surface of SiCN 200 °C was mostly dominated by Si–O bonds after N_2 plasma activation. The bond strength of SiCN 200 °C was $\sim$1.4 J m^{-2}, much weaker than the $\sim$2.3 J m^{-2} of SiCN 370 °C. By TEM and EDS analysis, the intermediate layer for 200 °C was observed to be much thicker than that for the 370 °C process. Moreover, it is found that the direct bonding for 200 °C is governed by SiO_2-to-SiO_2 direct bonding, explaining the weaker bond strength as compared to the general SiCN bond strength. Especially, as reported in our past studies, it was demonstrated that Si–C bonds formation at deposition and breakage by plasma activation are linked to the solid bond strength for SiCN direct bonding in this study.

Acknowledgments

The authors are grateful to imec's 3D team for valuable input and discussion. The author (FN) thanks the DS&T division of The Electrochemical Society for the grant received to present this work at the 2020 PRIME meeting.

ORCID

F. Nagano https://orcid.org/0000-0001-5315-8694

References

1. E. Beyne, *IEEE Design & Test*, **33**, 8 (2016).
2. S. W. Kim, L. Peng, A. Miller, G. Beyer, and E. Beyne, *IEEE International 3D Systems Integration Conference (3DIC)*,TS7.2 (2015).
3. G. Vakanas et al., *Microelectron. Eng.*, **140** (2015).
4. C. F. Tseng, J. G. Duh, and S. Y. Tsai, *Proceedings 2010 11th International Conference on Electronic Packaging Technology and High Density Packaging, ICEPT-HDP* (2010).
5. P. Y. Chia, A. S. M. A. Haseeb, and S. H. Mannan, *Materials (Basel).*, **9** (2016).
6. K. Zeng, R. Stierman, T. C. Chiu, D. Edwards, and K. N. Tu, *J. Appl. Phys.*, **97** (2005).
7. W. Peng, E. Monlevad, and M. E. Marques, *Microelectron. Rel.*, **47** (2007).
8. E. Beyne et al., *IEEE International Electron Devices Meeting (IEDM)*,32.4 (2018).
9. Y. Kagawa et al., *IEEE International Electron Devices Meeting (IEDM)*8.4 (2016).
10. H. Baumgart, T. J. Letavic, and R. Egloff, *Philips Journal of Research*, **49** (1995).
11. T. Tabata, L. Sanchez, V. Larrey, F. Fournel, and H. Moriceau, *Microelectron. Rel.*, **107** (2020).
12. S. Kühne and C. Hierold, *Procedia Engineering*, **5** (2010).
13. D. Diehl et al., *Microelectron. Eng.*, **92** (2012).
14. H. Takagi and R. Maeda, *Journal of Crystal Growth*, **292** (2006).
15. R. He, M. Fujino, M. Akaike, T. Sakai, S. Sakuyama, and T. Suga, *Appl. Surf. Sci.*, **414**, 163 (2017).
16. C. Wang and T. Suga, *Microelectron. Rel.*, **52** (2012).
17. B. Bayram, O. Akar, and T. Akin, *Diamond and Related Materials*, **19** (2010).
18. H. Takagi, R. Maeda, and T. Suga, *Sensors and Actuators A*, **105** (2003).
19. F. Mu, K. Iguchi, H. Nakazawa, Y. Takahashi, M. Fujino, R. He, and T. Suga, *Applied Physics Express*, **9**, 081302 (2016).
20. S. Iacovo, L. Peng, A. Phommahaxay, F. Inoue, P. Verdonck, S. W. Kim, E. Sleeckx, A. Miller, G. Beyer, and E. Beyne, *2019 IEEE 69th Electronic Components and Technology Conference (ECTC), Las Vegas, NV, USA*, p. 2206 (2019).
21. F. Inoue et al., *ECS Journal of Solid State Science and Technology*, **8** (2019).
22. J. Utsumi, K. Ide, and Y. Ichiyanagi, *Micro and Nano Engineering*, **2** (2019).
23. C. T. Ko and N. Chen, *Microelectron. Rel.*, **52**, 302 (2012).
24. S. Peter, S. Bernütz, S. Berg, and F. Richter, "FTIR analysis of a-SiCN:H films deposited by PECVD." *Vacuum*, **98** (2013).
25. I. Blaszczyk-Lezak, A. M. Wrobel, and D. M. Bielinski, *Thin Solid Films*, **497** (2006).
26. W. Kafrouni, V. Rouessac, A. Julbe, and J. Durand, *Appl. Surf. Sci.*, **257** (2010).
27. G. Mera, R. Riedel, F. Poli, and K. Müller, *J. Eur. Ceram. Soc.*, **29** (2009).
28. Y. Awad, M. A. ElKhakani, C. Aktik, J. Mouine, N. Camiré, M. Lessard, M. Scarlete, H. A. Al-Abadleh, and R. Smirani, *Surf. Coat. Technol.*, **204** (2009).
29. S. W. King, M. French, J. Bielefeld, and W. A. Lanford, *J. Non-Cryst. Solids.*, **357** (2011).
30. P. Gao, J. Xun, Y. Piao, W. Ding, D. Wang, X. Deng, and C. Dong, *Surface & Coatings Technology*, **201** (2007).
31. X. C. Xiao, Y. W. Li, L. X. Song, X. F. Peng, and X. F. Hu, *Applied Surface Science*, **156** (2000).
32. F. Inoue, A. Jourdain, L. Peng, A. Phommahaxay, J. De. Vos, K. J. Rebibis, A. Miller, E. Sleeckx, E. Bayne, and A. Uedono, *Applied Surface Science*, **404** (2017).
33. F. Inoue et al., *Microelectron. Eng.*, **167** (2017).